Electronic Supplementary Material (ESI) for Journal of Materials Chemistry C.

Supporting information

Organic nanowire waveguide exciton-polariton sub-microlaser and its photonic application

Qing Liao[a,b*], Zhenzhen Xu[b,c], Xiaolan Zhong[d], Wei Dang[e], Qiang Shi[b], Chao Zhang[d], Yuxiang Weng[e], Zhiyuan Li[d] and Hongbing Fu[a,b*]

[a] Beijing Key Laboratory for Optical Materials and Photonic Devices, Department of Chemistry, Capital Normal University, Beijing 100048, P. R. China

[b] Beijing National Laboratory for Molecular Science, Institute of Chemistry, Chinese Academy of Sciences, Beijing 100190, P. R. China

[c] The University of Chinese Academy of Sciences, Beijing 100039, P. R. China

[d] Laboratory of Optical Physics, Institute of Physics, Chinese Academy of Science, Beijing 100190, P. R. China

[e] Key laboratory of Soft Matter Physics, Institute of Physics, Chinese Academy of Sciences, Beijing 100190, P. R. China

*E-mail: hongbing.fu@iccas.ac.cn; liaoqing@cnu.edu.cn

1. Synthesis of CDSB.

The compound used in our work, 1,4-chloride-2,5-di[4'-(methylthio)styryl]- benzene (CDSB) was synthesized according to ref. 13 in the manuscript. All starting materials were purchased from Sigma-Aldrich and used as received without further purification. The tetrahydrofuran (THF, HPLC grade) and hexane were purchased from Beijing Chemical Agent Ltd., China. Ultra-pure water with a resistance of 18.2 MΩ·cm^{-1}, produced by using a Milli-Q apparatus (Millipore), were used in all experiments. Alumina membranes with a pore size of 20 nm and polytetrafluoroethylene filters (PTFE, Puradisc 25 TF, 0.1 μm) were bought from Whatman International Ltd.

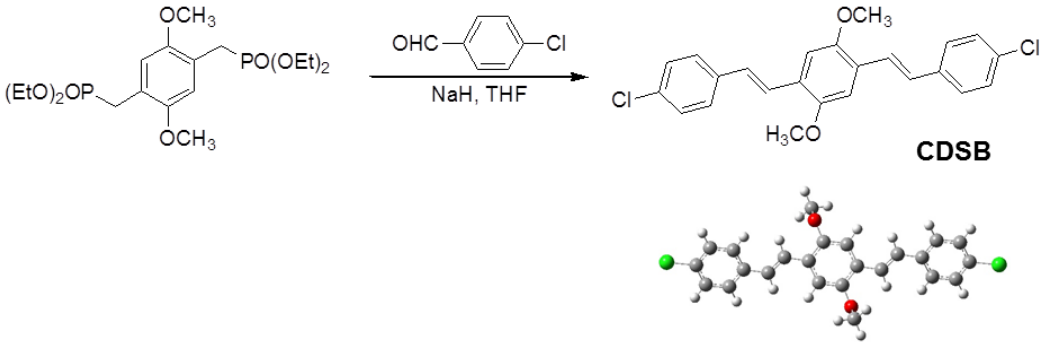

Scheme S1 Synthesis step of CDSB.

To a mixture of 2,5-bismethoxy-1,4-xylene-bis(diethyl phosphonate) (1.01 g, 2.26 mmol) and the 4-chlorobenzaldehyde (0.69 g, 4.52 mmol) in THF cooled in an ice bath was added 2 eq. NaH in small portions during a 30 min period. The reaction mixture was stirred at room temperature for 3 h and poured into water. The phase was extracted with CH_2Cl_2. The pooled organic phases were washed with water, dried over anhydrous $MgSO_4$, filtered, and evaporated. The product was separated by flash chromatography on silica gel by means of CH_2Cl_2/petroleum ether (1:4). And CDSB was obtained as a mixture of three isomers. Then the mixed product was dissolved in the minimum amount of a boiling solution containing iodine in toluene (0.1 mM) and refluxed for 12 h. After gentle removal of solvent in vacuum the green residue was further purified by flash chromatography on silica gel by means of CH_2Cl_2/petroleum ether (1:4). Finally a highly fluorescent light-green powder was obtained as the title compound (0.88 g, 2.03 mmol) in 90% yield. ^{1}H NMR (300 MHz, $CDCl_3$): δ 7.49-7.43 (m, 10 H), 7.11 (d, J = 16.4 Hz, 2 H), 7.11 (s, 2 H), 3.92 (s, 6 H, -OCH_3); MS (EI): 410.

2. Preparation and characterization of CDSB ONWs.

Preparation of single-crystalline ONWS of CDSB. ONWs of CDSB were prepared using a re-precipitation method by injecting 100 μL of a stock solution (5 mM) in THF into 2.0 mL of hexane under stirring, and aged for 3 hours.

Structural and optical characterization. The morphologies and sizes of ONWs were examined using field emission scanning electron microscopy (FESEM, Hitachi S-4300) at

acceleration voltages of 10-15 kV. Prior to analysis, the samples were coated with a thin platinum layer using an Edwards Sputter Coater. TEM images were obtained by a JEOL JEM-1011 transmission electron microscopy (TEM). One drop of the as-prepared colloidal dispersion was deposited on a carbon-coated copper grid, and dried under high vacuum. TEM measurement was performed at room temperature at an accelerating voltage of 100 kV. Atomic force microscopy (AFM, Veew NanoScope IIIa, Veew Co.) image is recorded in tapping mode using antimony doped silicon tip. The samples were prepared by casting the colloidal suspension on a silicon substrate, followed by drying in air for 2 hours. The X-ray diffraction (XRD) patterns were measured by a D/max 2400 X-ray diffractometer with Cu Kα radiation (λ=1.54050 Å) operated in the 2θ range from 3° to 30°, by using the samples of nanoparticle or SMCS filtered on the surface of an AAO membrane.

The diffused reflection absorption and emission spectra were measured on Shimidazu UV-3600 UV-VIS-NIR and Horiba FluoroMax-4-NIR spectrophotometers, respectively. The fluorescence quantum yield (Φ) was measured absolutely by using an integrating sphere.

3. Polariton lasing experiments on the ONWs.

Single ONW was investigated at room temperature in air by a home-made optical microscopy equipped with a 50×0.9 NA excitation objective. The samples were prepared by placing a drop of dispersion onto a glass substrate, which was then transferred on the 2D-movavble sample table of the optical microscope. The second harmonic (400 nm, 150 fs, 1 kHz) of a regenerative amplifier (Spitfire, Spectra Physics) seeded with a mode-locked Ti:sapphire laser (Tsunami, Spectra Physics) was focused to a 50-μm-diameter spot to excite the selected ONW wholly. The pump intensity of the pulse laser varied using a series of metallic neutral density filters. Then PL spectra were collected underneath by using a 50×0.9 NA objective that was mounted a 3D movable stage. A 430-nm long-wave pass dielectric filter was used to block any scattered excitation light. Finally the collected PL was coupled to an optical fiber and detected using a liquid-nitrogen-cooled CCD (SPEC-10-400B/LbN, Roper Scientific) attached to a polychromator (Spectropro-550i, Acton Research Corp.). The spectral resolution is 0.1 nm. If necessary, we could record the spatially resolved PL spectra along the body of the selected ONW with a spatial resolution about 2~3 μm, by placing an aperture (60 μm) in front of the optical fiber at the expense of PL collection efficiency. Using the same detection geometry, time-resolved PL was detected with a streak camera (C5680, Hamamatsu Photonics) dispersed by a polychromator (250is, Chromex) with a spectral resolution 1 nm and a time resolution 10 ps.

The experimental setup for the femtosecond time-resolved transient fluorescence spectroscopy based on non-collinear optical parametric amplification (NOPA) has been described in detail in ref. 28 in the main text. Briefly, the 800 nm fundamental beam of a Ti:sapphire amplifier laser (Spectra Physics) with 1 KHz repetition was split into two beams. One beam after second

harmonic generation (SHG) was used to excite the fluorescence of the samples. The bean size at the focal point was about 100 μm, which would cover several nanowires. Another beam after SHG was used as the fluorescence gating pulse. The fluorescence was seeded into a 2 mm beta barium borate (BBO) crystal, and then amplified by the gating pulses. The time delay between the excitation and the gating pulses was controlled a translation stage, and the amplified fluorescence signals were recorded by a CCD (Princeton Instrument) interfaced to a computer.

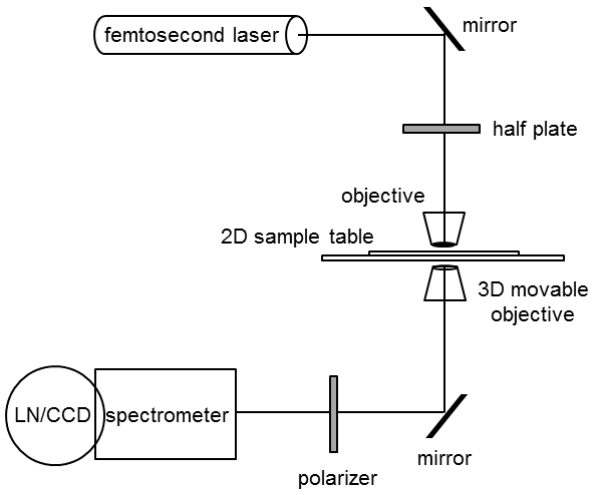

Scheme S2 Schematic of optical setup used for spatially resolved single CDSB ONW PL imaging and spectroscopy. The polarization of the excitation laser is regulated using half plate, while the polarization of output-lasing emission is measured using polarizer.

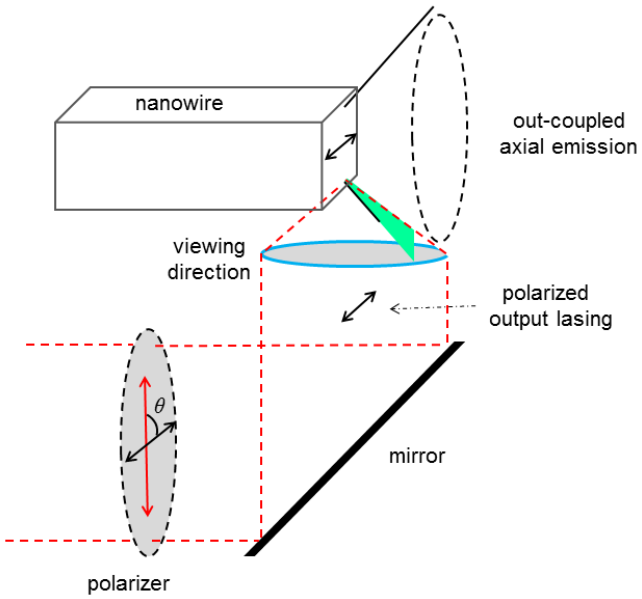

Scheme S3 Schematic of optical setup used for measuring the polarized output lasing from the ends of ONW. The black arrows are the polarized direction of output lasing, and the red arrow is the plane of the polarizer.

4. Structure analysis of CDSB ONWs.

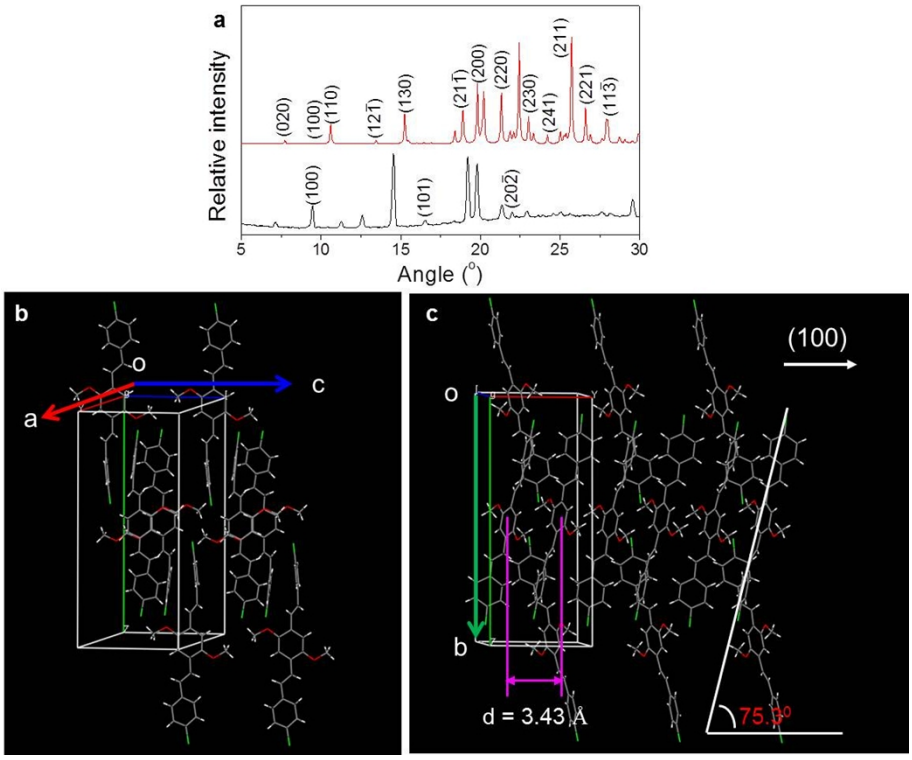

Figure S1. (a) XRD patterns of ONWs (black) of CDSB and the powder (red) simulated based on single-crystal data. Molecular packing arrangements of CDSB molecules in the ONWs along c axial (b) and a axial (c). The cell parameters of monoclinic CDSB crystal is a = 9.6685 (19) Å, b = 22.865 (5) Å, c = 9.6903 (19) Å, $\alpha = \gamma = 90°$, and $\beta = 112.41°$. In general, XRD "see" the crystal planes parallel to the supporting substrate, while ED "see" the crystal planes perpendicular to the supporting substrate. Combining XRD and SAED observations together, we concluded that ONWs grow preferentially along the [100] direction. The space of π-π stacking is 3.43 Å along a axial and in which CDSB molecules stack at a tilting angle of 75.3° along the nanowire Z-direction.

5. Absorption and Fluorescence of CDSB molecules and ONWs.

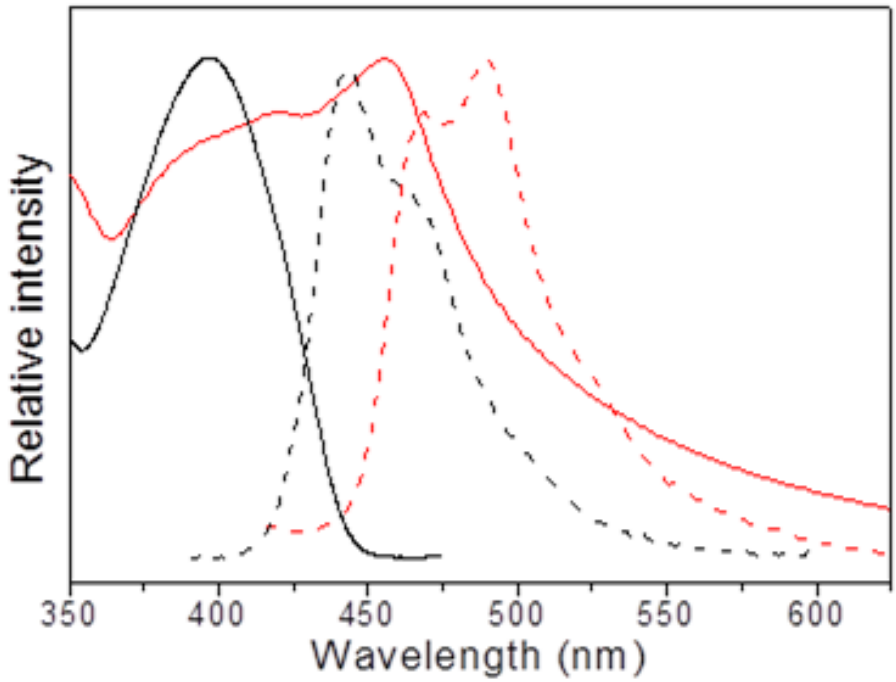

Figure S2. Steady-state absorption (solid) and fluorescence (dash) spectra of CDSB molecules in THF solution (black) with the concentration of 1.0×10^{-5} M, and diffused reflectance absorption (solid) and PL (dash) spectraof a 100-nm-thick film of CDSB (red) prepared by physical vapor deposition. The PL spectrum (red dash) displays three broad spontaneous emission bands at 465, 490 and 525 nm, corresponding to 0–0, 0–1, and 0–2 emissions, respectively.

6. The polarization dependence relationship.

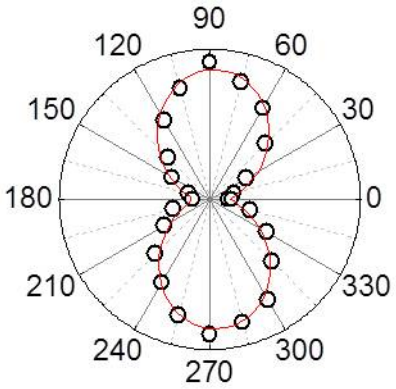

Figure S3. The polarization dependence of WGEP lasing emission as a function of angle θ between the X-direction and the polarizer (also see Scheme S3).

7. The assignment of the ONW cavity length.

We assigned the ONW length as the FP cavity length according to several evident points below:

Firstly, we were referring to the reported literatures such as *Phys. Rev. Lett.* **2010**, 105, 67401; *Adv. Mater.* **2011**, 23, 3659; *JACS* **2011**, 133, 7276.

Secondly, we calculated the modes in our ONWs using FDTD methods. The lateral size of our ONW could allow many types of modes in the cavity, and each mode is characterized by the propagation constant k_z and the lateral modal profile, whether for fundamental mode or for other higher order modes. The phase accumulation of each mode under a single round-trip is always $2 \cdot k_z \cdot L$. We had assigned these modes to TE polarization according to polarized measurement. At the same time, our experimental results showed that the perfect period resonant peaks (Figure 2c of our manuscript and Figure S4 below) had the regulated spacing, which should come from one mode resonance with the cavity. It suggested that only one mode could satisfy the resonance condition and occur in the cavity. Therefore, it is reasonable that the lowest order TE mode can occur in the cavity. In fact, this assumption is further supported from the energy point of view. Although there can exist many modes in the ONW cavity, the fundamental mode has the highest reflection coefficient upon the two facets of the cavity and thus lowest loss because its modal profile has the energy most strongly localized at the center of ONW compared with other high order modes. In comparison, higher order modes will endure larger reflection loss at each time impinging upon the ONW facet. Therefore, it is reasonable to only consider the fundamental mode in ONW.

Thirdly, we estimated the cavity length from our experimental data. The refractive index of a 110-nm-thick film of CDSB is determined to be 1.81±0.15 at the nonresonant range based on ellipsometry measurement (Figure S3a). Then the values (n-λdn/dλ) were calculated according to the literature (J. Voigt, *et al.*, *Phys. Stat. Sol. (b)* **1976**, 75, 213.) and were plotted in Figure S3b (black solid line). At the same time, we also used the equation (n-λdn/dλ= $\lambda^2/2L\Delta\lambda$) to calculate the values (n-λdn/dλ) of our ONWs based on experimental results. Here, L is assigned to the length of simplest FP cavity. We found the experimental results (n-λdn/dλ) of ONWs are compared with that of CDSB film. This indicated that it is reasonable for our assignment of cavity length.

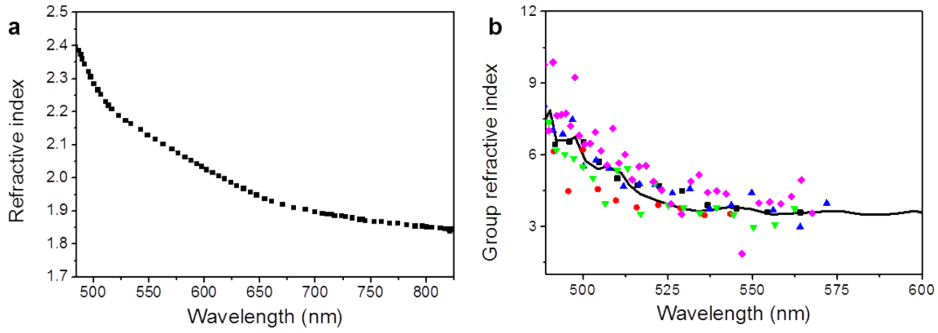

Figure S4. (a) The plot of refractive index-wavelength of the experimental results based on ellipsometry measurement. (b) The relationship of group index (n-λdn/dλ) and wavelength of 110-nm-thick film of CDSB (black solid line) and the experimental results of ONWs with different lengths.

8. The calculation of Kz.

The following procedure is use to fit the parameters in the dispersion curve and determine the k_z [Lambert Karel van Vugt, Optical Properties of Semiconducting Nanowires (Universal press, 1977)]. The dispersion curve is given by the equation (ref. 16 and 17 in our manuscript):

$$\hbar ck = \hbar ck_0 + \sqrt{\varepsilon b} * \omega \ * (1 + \frac{\Delta^2}{\omega * ((\omega_T - \omega))})$$

Initially we do not know the kz values of each data point, but we do know the Δk_z values between them which is $\Delta k_z = \pi/L$, where L is the length of nanowire. So all the k_z points are determined to a constant k_{z0} and, this constant is determined from the nonlinear fitting of the dispersion curve. Finally, the fitted $\sqrt{\varepsilon_b}$ = 1.8, which is close to the experimental values determined from ellipsometer measurements. We obtain the coupling Δ from this nonlinear fitting.

Polariton dispersion.

The eq (1) in the main text can be rewritten as

$$\begin{pmatrix} E_{ph} & V \\ V & E_{ex} \end{pmatrix} \begin{pmatrix} \alpha \\ \beta \end{pmatrix} = E \begin{pmatrix} \alpha \\ \beta \end{pmatrix} \qquad (1)$$

Here E_{ph} and E_{ex} are the energies of the uncoupled cavity photon and the bare exciton, respectively, and V represents the interaction the potential between them. E are the new eigenvalues of the coupled system with $|\alpha|^2$ and $|\beta|^2$ of the mixing coefficients of the cavity photon and the exciton, respectively. Because of eqs. (2) and (3),

$$\begin{pmatrix} E_{ph} - E & V \\ V & E_{ex} - E \end{pmatrix} = 0 \qquad (2)$$

$$E_{ph} = \frac{hck_z}{\sqrt{\varepsilon_b}} \qquad (3)$$

$$\frac{hck_z}{\sqrt{\varepsilon_b}} = \left(\frac{V^2}{E_{ex} - E} + E \right) \quad (4)$$

where h is the plank constant, c is the speed of light in the vacuum, k_z is the wavevector, and $\varepsilon_b = 3.24$ is the background dielectric constant ($n = \sqrt{\varepsilon_b}$), one can obtain eq. (4). As shown below in Table S1, good fits to polariton dispersion (Fig. 2 in the main text) were obtained following eq. (4) with E_{ex} = 2.72~ 2.87 eV, which corresponds to the energy range of 0–0 excitons (see Fig. 2c in the main text). Moreover, the coupling strength of V was determined to be 0.355 ~ 0.617 eV (Table S1), giving rise to a Rabi splitting energy of $\Omega = 2V$ = 0.71 ~ 1.23 eV. The value of Ω is about 26% ~ 43% of the exciton resonance energy, suggesting that strong coupling regime is achieved in our system.

According to equation (1) and $|\alpha|^2 + |\beta|^2 = 1$, the photonic $|\alpha|^2$ and excitonic $|\beta|^2$ fractions of LPB can be calculated as a function of kz.

E_{ex} (eV)	V (eV) = Ω/2	R-Square
2.72	0.35469	0.988755
2.73	0.37400	0.991415
2.74	0.39288	0.993494
2.75	0.41140	0.995120
2.76	0.42962	0.996387
2.77	0.44756	0.997369
2.78	0.46527	0.998121
2.79	0.48277	0.998685
2.80	0.50009	0.999097
2.81	0.51724	0.999384
2.82	0.53424	0.999567
2.83	0.55110	0.999665
2.84	0.56785	0.999691
2.85	0.58448	0.999658
2.86	0.60101	0.999575
2.87	0.61745	0.999452

Table S1 The calculated results following eq.(1) in the main text with different values of E_{ex}. The results show that the fit results is reasonable when the parameter E_{ex} in the range of 2.72-2.87 eV, corresponding to 0–0 excitons.

9. Compare between PL spectra below and above threshold for an ONW.

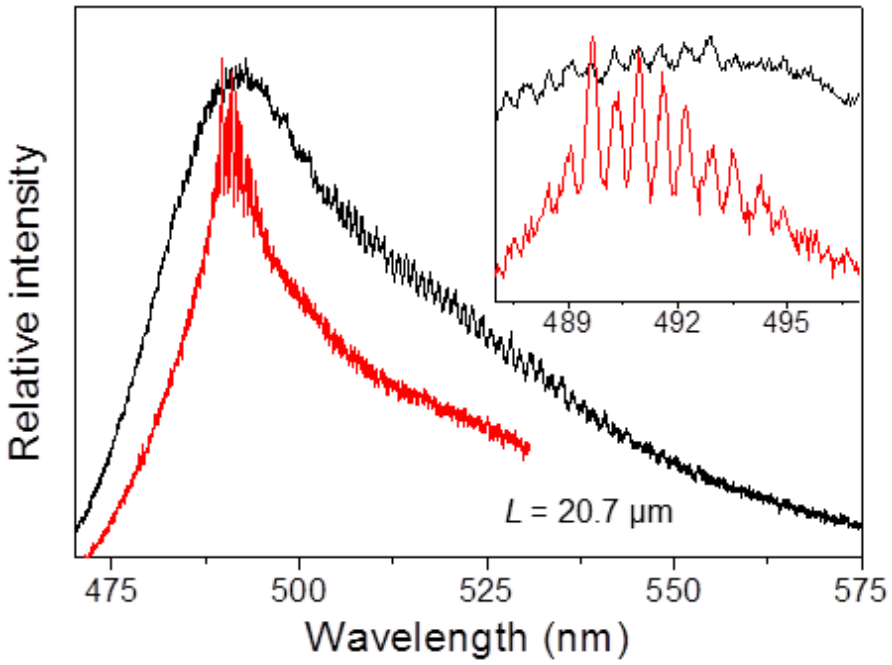

Figure S5. The spectra of spontaneous polariton emission (black line) below threshold and polariton lasing emission (red line) above threshold. Here, the length of the chosen ONW is 20.7 μm. Inset shows the amplificatory spectra in the range of 478-502 nm. It indicates that polariton lasing happens at the largest gain positions. Moreover, almost identical FP cavity resonances are observed for the same ONW polariton laser below and above threshold, indicating strong coupling regime remains under both conditions

10. The comparison of the dynamic behaviors at the different wavelengths.

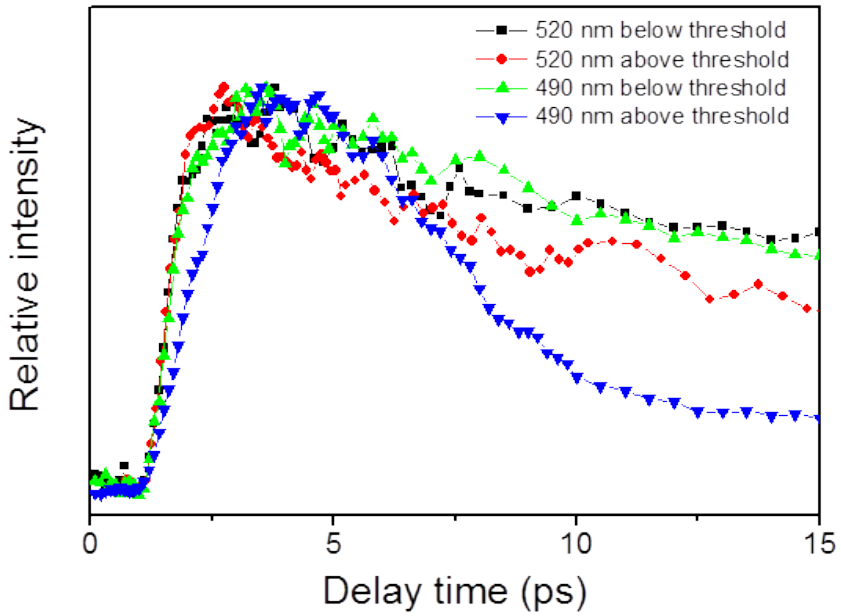

Figure S6. The dynamic curves below and above threshold at 490 nm and 500 nm. Importantly, the clear lasing process can be seen from NOPA experiments, which is different to spontaneous emission. As shown in Figure 1s below, the profiles of dynamic curves are very similar below and above threshold at 520 nm (black and red lines). They have the same rising edge, and the faster lifetime of the case above threshold is due to the influence of bimolecular quenching. However, the situation of the photoluminescence at 490 nm is big different. Above threshold, the rising edge of dynamic curves becomes slower because of the formation of stimulated process (green and blue lines). At the same time, the collapse of the emission lifetime shows the Gaussian profile different to the decay curve of common spontaneous emission, which strongly supports the fact of the formation of lasing behaviors.

11. Numerical calculations of CDSB ONW waveguide cavities.

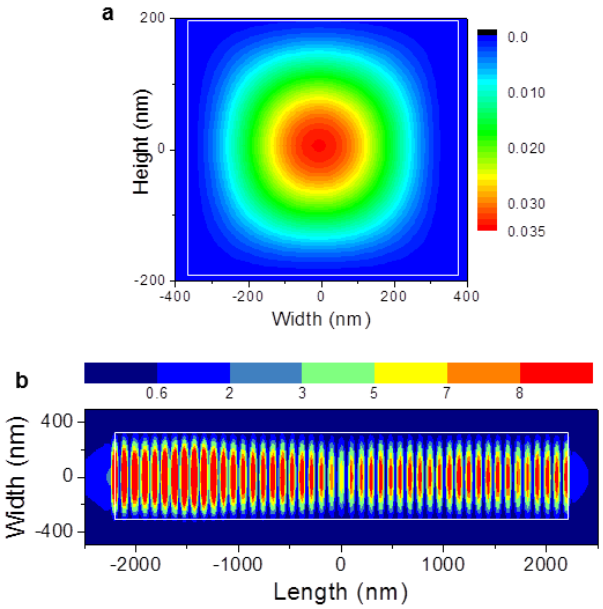

Figure S7. (a) and (b) Two-dimensional projection of the obtained three-dimensional electric-field intensity distribution at 490 nm in the ONW (4.5-μm-long, 750-nm-wide and 400-nm-high) on a silica substrate. The simulation domain is 1600 nm×6900 nm×1000 nm. In order to avoid the reflection when the light arrives at the simulation boundary, we take the perfect matched layer (PML) as the boundary condition, thus the EM wave which arrives at the simulation boundary would be absorbed completely. The grid size is 20 nm×20 nm×20 nm and the time step satisfies the courant stability condition. The light radiates from a slab excitation to illuminate the structure from one side of the waveguide. We use the fundamental eigenmode (lowest order) of the waveguide as the incident light. The wavelength is 490 nm.

12. Optical loss, α, of a single ONW waveguide.

Optical propagation losses for single ONWs were determined by monitoring the intensity out-coupled at the tip of a ONW while translating a highly focused laser excitation spot (2 μm diameter, ~ 10 nJ/cm^2) along the wire length. The origins of the optical loss were attributed to (i) re-absorption, as seen Fig. S2, (ii) propagation losses at grain boundaries arising from imperfect crystalline, (iii) the relatively low refractive index of the CDSB material, and (iv) substrate coupling losses that occur due to the asymmetric waveguide format of the nanowire devices.

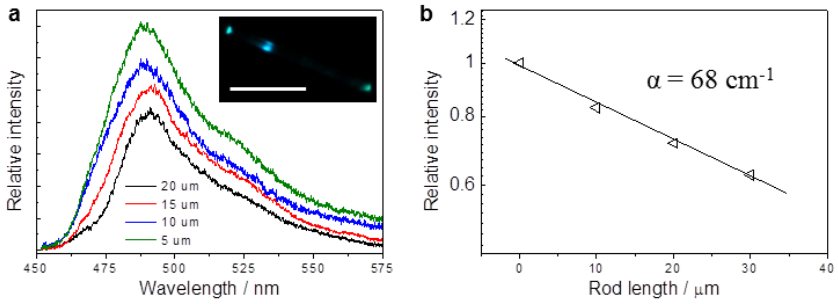

Figure S8. (a) Spatially resolved PL spectra of out-coupled light for an ONW recorded by excitation at a different distances from the tips. Inset shows the corresponding fluorescence micrograph. The scale bar is 10 μm (b) The logarithmic plot of relative intensities of emission peak for an ONW versus excitation position for the emission spectra. The corresponding fit curves are shown as black as solid lines. Propagation loss are determined to be 68 cm^{-1} based on equation, $\alpha = \log(I_{out}/I_{in})L^{-1}$, where I_{in} and I_{out} are the intensities of incidence and out-coupled light, respectively, and L is the propagation distance.

13. Waveguide output of polarization dependence of a dendritic structure.

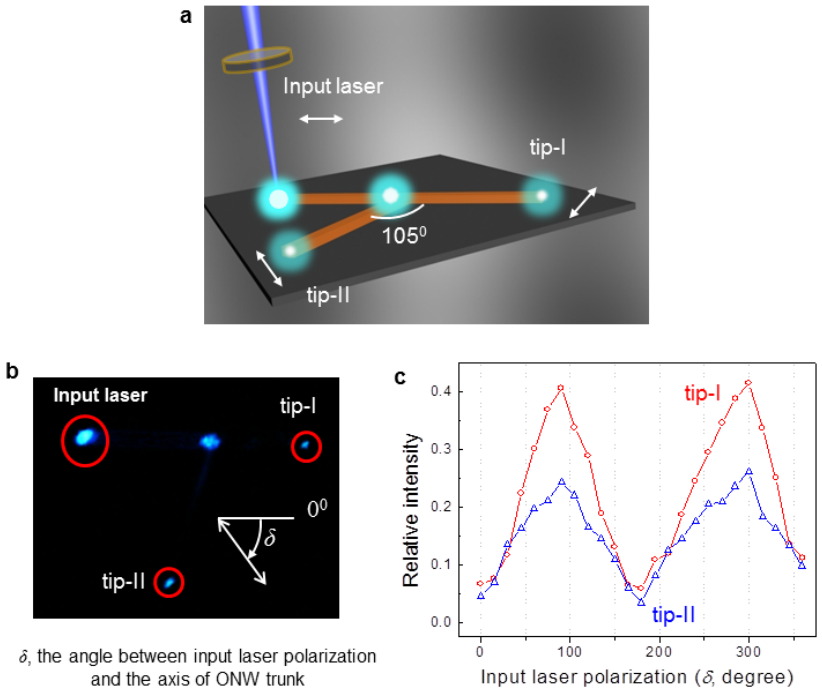

Figure S9. (a) A Schematic illustration of a dendritic structure excited by focused polarized laser. (b) PL micrograph of the dendritic structure. The excitation point, tip-I and tip-II are marked by red circles. The angle δ is according to the angle between excitation laser polarization and the longitudinal direction of the trunk of the dendritic structure. (c) The output lasing intensities at the tip-I (red circle) and tip-II (blue triangle) as a function of angle δ.